Structural features of neat 5-hydroxymethylfurfural (HMF) in the liquid state

Giulia Adriana Bracchini [a,1], Emanuela Mangiacapre [b,1], Fabrizio lo Celso [a,c],
Daniel J.M. Irving [d], Carlo Ottaviani [a], Grazia Isa C. Righetti [e], Maria Enrica Di Pietro [e],
Andrea Mele [e], Lorenzo Guazzelli [f], Olga Russina [a,b], Alessandro Triolo [a,*]

[a] *Istituto Struttura della Materia, Consiglio Nazionale delle Ricerche (ISM-CNR), Rome 00133, Italy*
[b] *Department of Chemistry, University of Rome Sapienza, Rome 00185, Italy*
[c] *Department of Physics and Chemistry, University of Palermo, Palermo, Italy*
[d] *Diamond Light Source Ltd., Didcot, Oxfordshire OX11 0QX, UK*
[e] *Department of Chemistry, Materials and Chemical Engineering, Politecnico di Milano, Milano, Italy*
[f] *Department of Pharmacy, University of Pisa, Via Bonanno 6, 56126 Pisa, Italy*

ARTICLE INFO

ABSTRACT

Here we investigate the local structural organization in liquid neat 5-hydroxymethylfurfural (HMF) by the synergic use of high energy X-ray scattering, NMR spectroscopy and molecular dynamics simulations, providing atomistic insight into the correlations that characterise HMF liquid state.

HMF has been acknowledged as one of the "sleeping giants" among those renewable compounds, with yet underexploited market potential. It can be obtained from renewable carbohydrate sources via a few consecutive steps and, due to its different functional groups, it can be potentially transformed into a plethora of compounds.

An adequate knowledge of the driving interactions into its liquid state can be of fundamental relevance in individuating successful solvents, where HMF can be dissolved, extracted and treated to deliver new compounds. As such, this study has then the potential to provide new, sustainable routes in HMF manipulation, alternatively to current methods.

The X-ray scattering validated MD study reveals the existence of a distinct π–π stacking arrangement, characterising the mutual ordering between neighbour HMF molecules. Further correlations involve hydrogen bonding between aldehyde and hydroxyl oxygen and hydroxyl hydrogen. Furthermore, indication of the existence of OH···π hydrogen bonding interaction has been detected.

An NMR strategy has been applied to confirm the existence of these mutual interactions, identifying the associated structural motifs.

These findings underscore the complex and heterogeneous nature of the structural organization of liquid HMF.

1. Introduction

The transition toward a sustainable development relies on the replacement of petroleum-based molecular building blocks with bio-based alternatives. To make such a transition feasible, e.g. by utilizing renewable starting materials for value-added activities and products, one must consider lignocellulosic biomass, which is produced by nature in over 200 billion tons per year [1], as the only realistically renewable feedstock option. Modern chemical research, therefore, is currently focusing on identifying platform chemicals, which can be synthesized from non-fossil precursors, typically agri-food biomass and related waste, and are easily ready to diverse chemical transformations.

In 2010, Bozell and Petersen critically revised the repertoire of platform chemicals from biorefineries, which were previously identified as the "Top 10" by the US Department of Energy (DOE) [2]. They highlighted the pivotal role of furan derivatives, such as furandicarboxylic acid (FDCA) and 5-hydroxymethylfurfural (HMF, (chemical structure and atom labels are reported in Scheme 1)), as

---
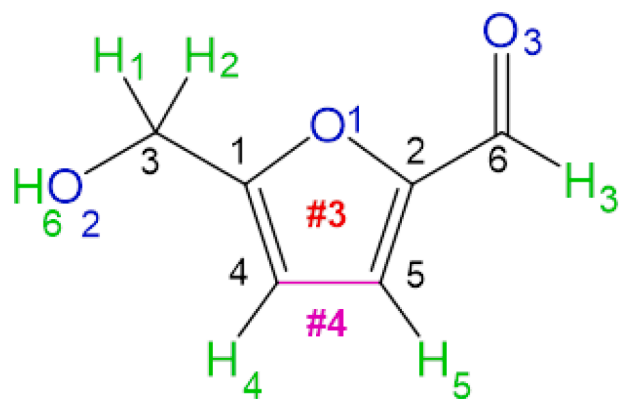
Scheme 1. Molecular formula and atom labels in 5-hydroxymethylfurfural (HMF). The colour code is introduced for clarity to identify the type of atoms discussed in the structural assessment: O atoms, potential H-bond acceptor sites, are in blue, H atoms, including OH and aldehyde H, are in green, the carbon skeleton in black. Virtual atoms are indicated as #3 and #4. They are located in the center of the aromatic five-membered ring and at the midpoint of the C4 – C5 bond, respectively. Their use is explained in the main text.

Table 1
HMF molar fraction corresponding to each NMR measurement.

Point	Solvent (uL)	χ_{HMF}^{a}	χ_{HMF}^{b}
1	0	1	1
2	10	0,95	0,97
3	20	0,91	0,94
4	30	0,87	0,91
5	40	0,83	0,88
6	50	0,80	0,85
7	150	0,57	0,66
8	250	0,44	0,54
9	400	0,005	0,008

(a) HMF molar fraction in CD3CN, (b) HMF molar fraction in DMSO-d_6.
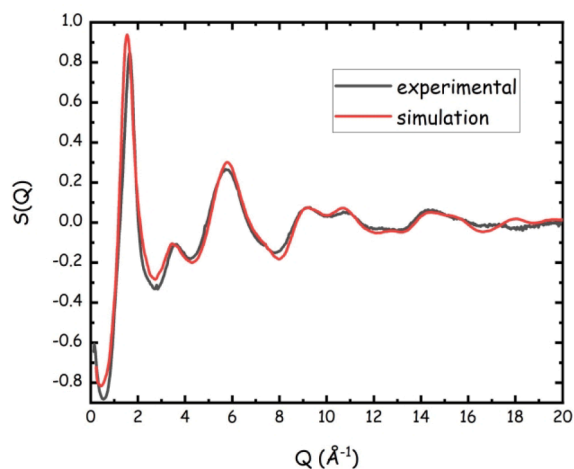

Fig. 1. Experimental (black line) and computed (red line) X-ray weighted normalised static structure factors for neat liquid HMF at 40 °C.

potential synthons for high-value processes, paving the way for 21st-century chemistry, free from fossil feedstock.

Indeed, HMF can be obtained from renewable carbohydrate sources via a few consecutive steps, which vary depending on the nature of the starting sugar employed. Using fructose represents the most direct access to HMF, although attention has been directed over time to more complex polysaccharides such as inulin, starch and cellulose [3–5]. In
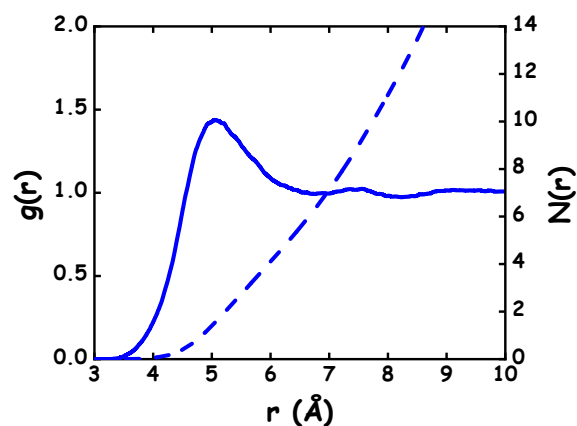

Fig. 2. MD-computed RDF (continuous line) and the corresponding running neighbour numbers (dashed line) of the ring centre for neat HMF at 40 °C.

the latter case, depolymerization of the polysaccharide backbone is required, followed by the glucose to fructose isomerization reaction, before the final dehydration step into HMF [6,7]. In the last few years, great research efforts have been devoted to exploring and optimizing the reaction conditions to convert sugars into HMF [8]. The use of neoteric solvents such as ionic liquids, deep eutectic solvents and low melting mixtures, mixtures of solvents or biphasic systems, different catalytic acidic systems, microwave and ultrasound has been investigated. [3,9–16]. Scale-up production of HMF has been implemented and industrial plants are present in Europe, North America, China and Japan [8].

What makes HMF particularly attracting, beyond its natural origin and abundance, is its potential transformation into a plethora of diverse compounds (see e.g. [17]). The impressive potential of HMF as a synthon in organic chemistry led to its metaphorical description as a "sleeping giant", ready to be awakened [18–21]. Indeed, HMF contains an aldehyde and a primary hydroxyl group on the opposite sides of the furan frame, which allow for the preparation of 175 different compounds and 20 polymers. 2,5-disubstituted furans obtainable from HMF, either by oxidation or reduction reactions, are clear possible monomers to produce bio-based polymers and are often referred to as the "sleeping giants" of the renewable compounds for their yet underexploited market potential [21]. 2,5-furan dicarboxylic acid (2,5-FDCA) is the most praised representative of this class of compounds and is already used for the production of 100 % bio-based polyethylene-furanoate (PEF), which is manufactured at the commercial-scale by several companies (BASF, Avantium and Eastman) [22].

More complex elaborations of the carbonyl and alcohol functional groups as well as of the furan ring are possible and allow enhancing the structural diversity achievable starting from HMF. For instance, aldol condensation, addition to the aldehyde and Diels Alder reactions gave access to biologically relevant compounds. Several examples have been reviewed elsewhere [23–26]. It is also worth mentioning, that HMF may allow to prepare benzene-based aromatic derivatives [27,28], thus representing with lignin the renewable option for this well-known class of compounds. All these aspects make HMF one of the most promising biomass-based platform chemicals.

However, the other side of this intriguing reactivity potential is the intrinsic lability of HMF at acid and basic conditions, its low thermal stability, and the occurrence of easily triggered side reactions. These effects might hinder the route to HMF-based sustainable processes. In particular, rehydratation to levulinic acid and formic acid or aldol condensation are often observed and represent the major hurdle to HMF widespread utilization. In particular, the end products of the aldol condensation reaction followed by cross linking are soluble and insoluble complex polymers, called humins. The mechanism of formation of humins, as well as their structures and level of agglomeration, are still
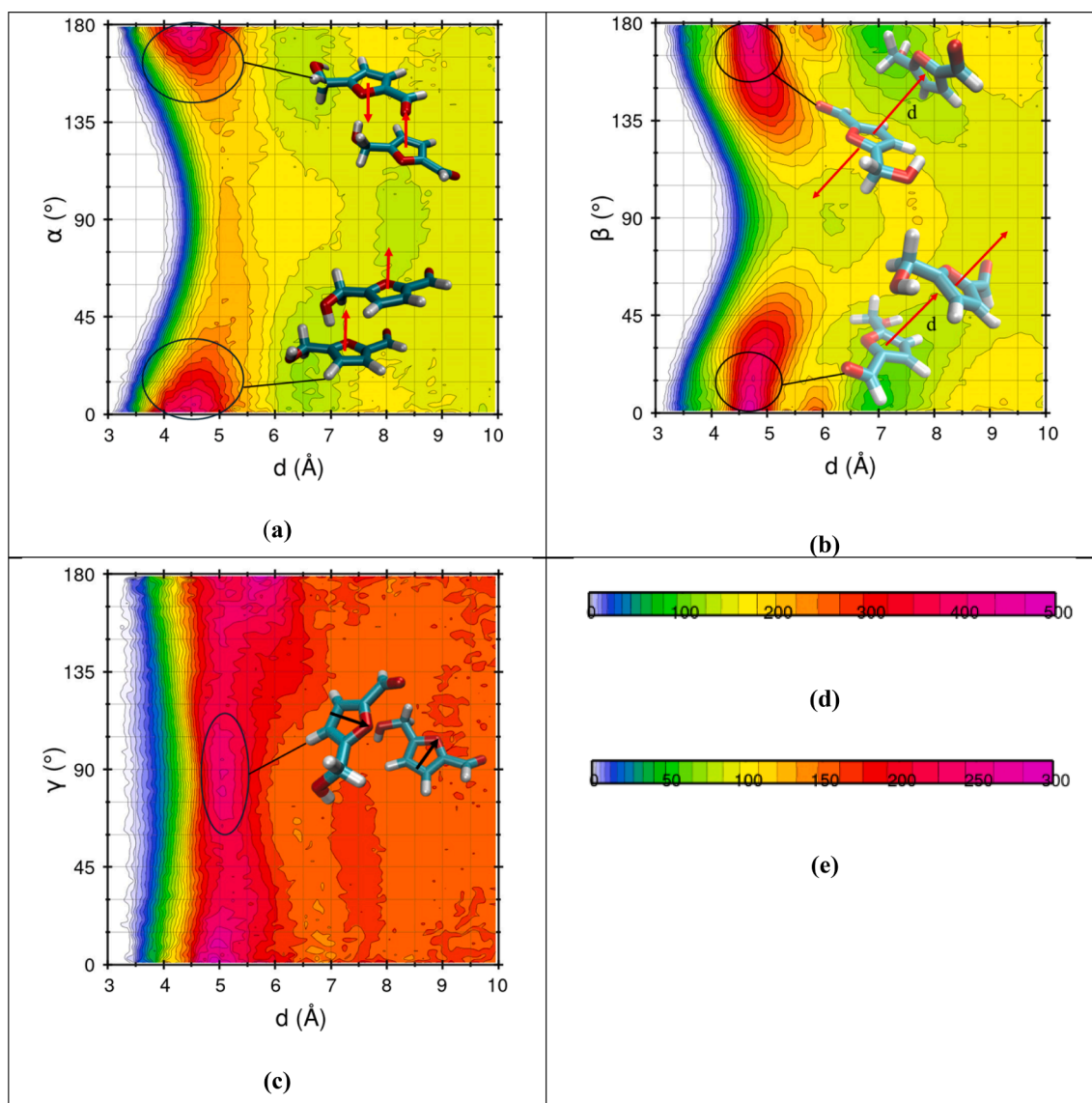
Fig. 3. Combined distribution functions for: a) the angle between the vectors perpendicular to the neighbour rings (α); b) the angle between the vector connecting neighbour ring centres and the vector perpendicular to the reference ring (β); c) the angle between the vectors with extremes the virtual atom #4 and ether oxygen O1 (γ), for the two neighbour rings, as functions of d, the distance between neighbour rings. Colour scale (d) in related to CDFs in a) and b), while colour scale (e) is referred to the CDF in c).

matter of investigation and depend on several parameters, such as temperature, reaction time, solvents, concentration, catalysts and so on [29,30]. Another issue encountered when dealing with the preparation of HMF is its recovery from the reaction solution: indeed, strong interactions with reaction media hamper the extraction and favour HMF degradation. In the search of possible options to overcome or, at least, limit humins formation and favour HMF extraction, the role played by the solvent has been questioned in recent years [31–35].

In this context, it is crucial to comprehend and rationalise how HMF interacts with traditional or neoteric sustainable solvents and how solvation dynamics of HMF occurs in diverse solvents (see e.g. [36]).

In the recent past, MD simulations were used to investigate water and water-DMSO solutions of HMF, highlighting the preferential solvation of DMSO towards HMF [37]. Aqueous solutions of HMF at ambient and hydrothermal conditions were investigated using MD simulations, to account for thermodynamic, structural and dynamic properties, as a function of water content, temperature and pressure. Therein, strong intermolecular HMF-HMF hydrogen bonding correlations were detected with respect to weaker interactions with water. Also, it was highlighted

that the furan ring oxygen is less involved in hydrogen bonding (HB) interactions than aldehyde or hydroxyl oxygen [38]. Neat HMF has been investigated using MD simulations, comparing different available classical potentials to extract information on its thermodynamic properties [39]. Therein, it emerged that among the probed force fields, no one succeeds in fully accounting for density and vapour liquid equilibrium properties. More recently, the role of anions in HMF solvation in selected ionic liquids was explored using MD simulations [10]; this work stimulated related report on the extraction of HMF from [C4mim][BF4], using THF [40].

In this work, we undertook a joint experimental and computational exploration of structure and solvation features in liquid neat HMF. The synergy between high energy X-ray scattering (HEXS) experiments and related MD simulations to access structural features at atomistic level is a well-established tool, as both techniques provide access to length scales of the order of Å/nm, which are the proper scale where microscopic and mesoscopic correlations occur (see e.g. [41]). The use of synchrotron-based HEXS allows rapid and clean data collection that ensures a very good quality of the data set to be used as a benchmark for
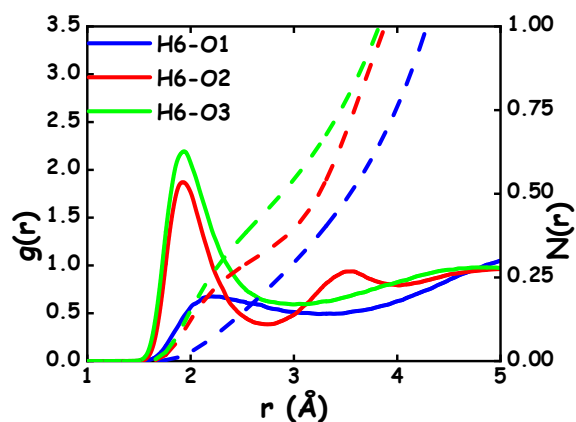
Fig. 4. Radial distribution functions (continuous lines) and corresponding running neighbour numbers (dashed lines) of hydrogen bond (HBs) correlations, H6···O1 (blue line), H6···O2 (red line), and H6···O3 (green line) in liquid HMF.

MD simulations. The latter can subsequently be used to extract atomistic details on the structural correlations driving the local order in the liquid state. The integration of these techniques with NMR spectroscopy on mixtures of HMF with different solvents allows probing local correlation phenomena and interaction forces in bulk liquid HMF and their evolution in the presence of selected molecular solvents used as disruptive agents, offering a reliable picture of the structure of liquid HMF.

Overall, in this work, we aim at providing a first insight into neat liquid HMF structure and mutual interactions, in order to be able to foresee and speculate on the nature of interactions with more complex solvents.

2. Materials and methods

2.1. Experimental details

The 5-hydroxymethylfurfural (HMF) sample used for X-ray experiments was an Apollo Scientific product with purity above 99.57 %, with a stated density at 20 °C of 1.243 g/cc. It is a brown solid that was kept in freezer, under no air or light exposure.

The solid sample was kept under argon and mildly heated until a brown liquid is obtained. Using a syringe, the liquid was transferred into a glass capillary that was later sealed with glue.

The 5-hydroxymethylfurfural (HMF, 98 %) sample used for NMR characterizations was purchased by Fluorochem; deuterated solvents were purchased by Merck. All reagents and solvents were used without any further purification. Pristine HMF was transferred in the NMR tube and heated at 40 °C until liquid. The ^{1}H NMR spectra of the concentrated HMF solutions, recorded at 313 K, were firstly recorded on the pure compound, then small amounts of solvent were added in the NMR tube as specified in Table 1. For the diluted samples, 5 mg of HMF were weighted in a vial, dissolved in 400 μL of deuterated solvent and transferred in the NMR tube. In all cases a coaxial insert containing the same deuterated solvent used for diluting HMF was used to ensure proper chemical shift reference. In DMSO-d_6, the signal at 0 ppm of tetramethylsilane (TMS) added in the coaxial insert was used to validate the referencing protocol.

2.2. NMR spectroscopy measurements

^{1}H NMR were performed at 313 K to ensure that all samples were in the liquid state. The spectra were recorded on a Bruker NEO 500 MHz spectrometer equipped with a direct observe BBFO (broadband including fluorine) iProbe and variable-temperature unit. The instrument was carefully tuned, shimmed and the 90° pulses calibrated. For all

the samples, ^{1}H NMR spectra were recorded with 16 scans and using 65,536 points. [1]H chemical shifts (δ) are given in parts per million (ppm) relative to the residual solvent peak within the coaxial insert. In DMSO-d_6, TMS was used as a crosscheck of the chemical shifts referencing protocol.

2.3. X-ray scattering measurements

X-ray total scattering data were collected using I15-1 XPDF at Diamond Light Source (UK) using an energy of 76.69 keV (0.161669 Å). Data were collected onto a Perkin Elmer XRD 4343CT at distance 700 mm, with beam stop mounted to the detector to allow for the collection of low angle scattering. The sample was loaded into glue sealed 2 mm borosilicate capillaries and loaded onto the beamline using the automated robot system. Measurements were collected for ca. 10 min in total with relevant backgrounds and empty capillary measurements collected for processing. The sample was measured at 40 °C using an Oxford Cryosystems Cobra.

Data were processed into 1D data using DAWN [42]. Corrections were applied for background, absorption, polarisation and Compton scattering using GudrunX [43].

2.4. Molecular dynamics

Molecular dynamics simulations were performed using the GROMACS 2021.3 package [44,45]. Bonded and non-bonded parameters for HMF were described using an all-atoms potential OPLS-AA force field [46]. The simulations were performed using a cubic box containing 1000 molecules; periodic boundary conditions were applied. Force field parameter files were created by LigParGen webserver [47–49]; initial configurations were created by Packmol software [50]. The starting density was fixed 10 % higher than the experimental one. The equilibration procedure was done in several steps, starting from a 2 ns NVT simulation at 400 K, followed by a series of 2 ns NPT runs lowering progressively the temperature to 353 K and then to 313 K at 1 bar. After the equilibration phase, the system was run for a total of 100 ns for a production run at 313 K, and then a trajectory of 2 ns was saved at a frequency of 1 ps for the calculation of the structural properties. Simulations were always checked versus the experimental density (density at 313 K fluctuates within 1 % around 1.205 g/cc, to be compared with experimental values of 1.243 g/cc at 293 K) and the energy profile. During the production runs, for the temperature coupling, a velocity rescaling thermostat [51] (with a time coupling constant of 0.1 ps) was used, while for the pressure coupling, we used a Parrinello–Rahman barostat [52] (1 ps for the relaxation constant). The Leap-Frog algorithm with a 1.0 fs time step was used for integrating the equations of motion. Cut-offs for the Lennard-Jones and real space part of the Coulombic interactions were set to 16 Å. For the electrostatic interactions, the Particle Mesh Ewald (PME) summation method [53,54] was used, with an interpolation order of 6 and 0.08 nm of Fast Fourier Transform grid spacing.

The X-ray weighted structure factor was computed together with selected pair correlation functions, angular distribution functions and spatial distribution functions using TRAVIS [55–57].

3. Results and discussion

Liquid 5-hydroxymethylfurfural (HMF) was preliminarily explored by high energy X-ray scattering, in order to access information on its local structural organization at atomistic level.

Fig. 1 reports a comparison between experimental static structure factor, S(Q), and the corresponding quantity obtained by MD simulation. The experimental data are characterized by the usual peaks alternation that is found in liquid systems, reflecting both intra-molecular (typically via covalent bonds) at high Q values and inter-molecular correlations at lower Q values. In particular, a strong peak is detected at ca. 1.6 Å^{-1},
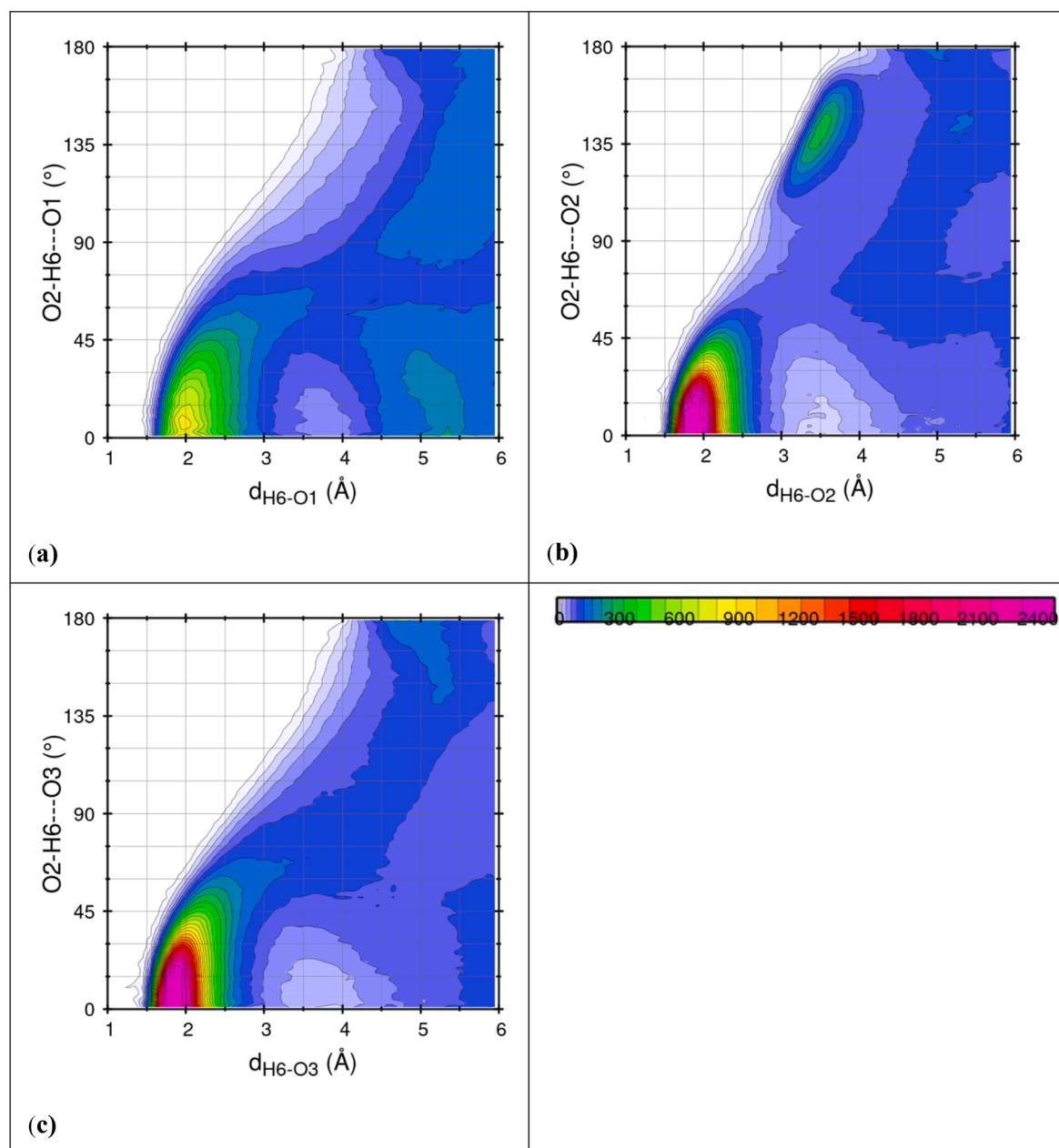
Fig. 5. Combined distribution functions for the angle O2-H6···O1 (a), O2-H6···O2 (b), and O2-H6···O3 (c) as functions of distances d_{H6-O1}, d_{H6-O2}, d_{H6-O3}, respectively.

which is related to first neighbor correlations. It is noteworthy that no scattering features are detected at lower Q values, indicating the absence of strong mesoscopic correlations in this liquid, similarly to our recent observations e.g. in anisole and its derivative [58]. Therefore, no mesoscopic spatial heterogeneities or clusters are formed, which are commonly encountered in other aromatic liquids [59], molecular "fragile" glass-forming liquids [60,61], ionic liquids [62,63], and deep eutectic solvents (DES) [64–67]. On the other hand, the peak at 1.6 Å^{-1} is associated with the existence of intermediate or medium range order, which is characteristic of organic liquids and reflects first-neighbor correlations.

We stress the close match between experimental and MD-derived structure factor, which represents a strong validation of the structural information extracted from MD simulations to provide atomistic insight into liquid HMF organization.

By inspection of MD-derived trajectories, we further explored the structural correlations in liquid HMF.

In Fig. 2, the Radial Distribution Functions (RDFs) (solid lines) and the corresponding running neighbor numbers (dashed lines) for the centers of the rings (#3 in Scheme 1) are illustrated.

HMF rings are structurally correlated: the RDF is characterized by a well-defined peak centered at ca. 5 Å with an amplitude larger than unity and a minimum at around 6.5 Å, where the number of first neighbors amounts to a value of approximately 6.

Clearly, rings correlations are fundamental in driving the local order in liquid HMF.

In order to better clarify how the interacting rings are mutually arranged, we evaluated a series of Combined Distribution Functions (CDF), shown in Fig. 3. These are color maps with abscissa representing the mutual ring centers distance, d, between neighbor HMF molecules and ordinates, respectively: a) the angle between the vectors perpendicular to the neighbour rings (α); b) the angle between the vector
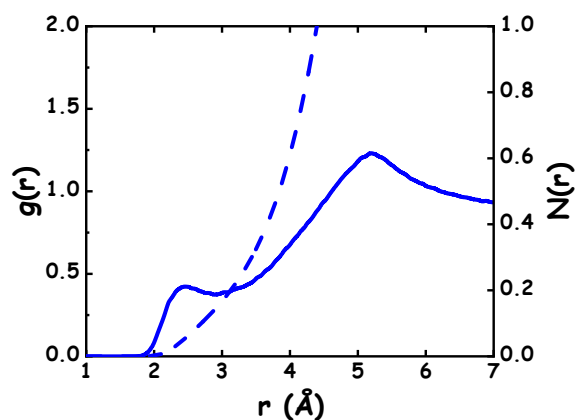
Fig. 6. RDF (continuous line) and the corresponding running neighbour numbers (dashed lines) for the H6···#3 correlation in liquid HMF.
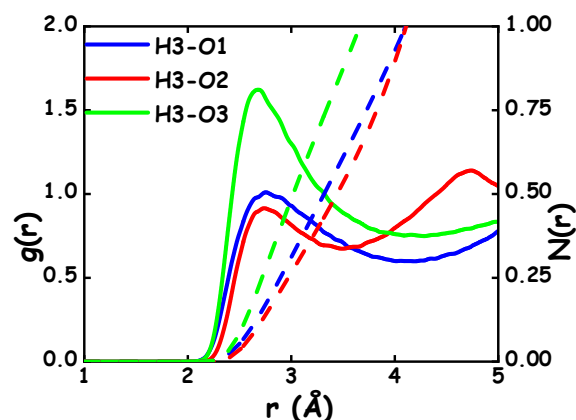

Fig. 8. MD-computed RDF (continuous line) and the corresponding running neighbour numbers (dashed line) of the correlation H3··O1 (blue line), H3··O2 (red line) and H3··O3 (green line) for neat HMF.

Table 2
Coordination numbers of HMF oxygen atoms around the aldehydic hydrogen (H3) as a reference site.

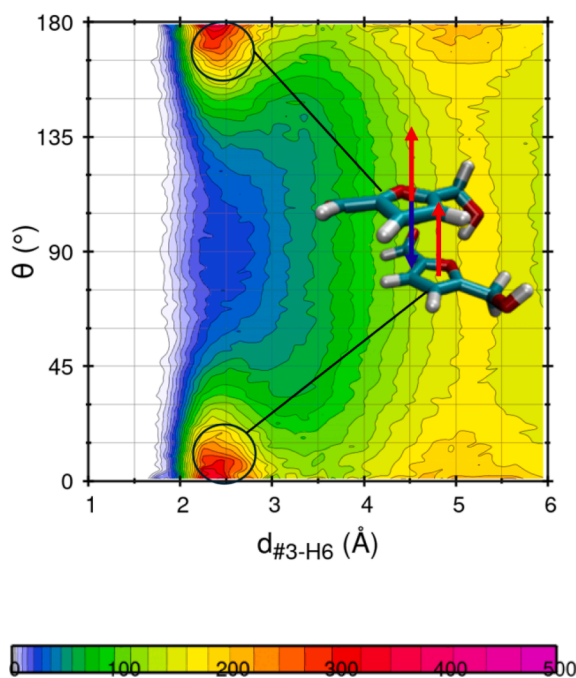| Correlation	R_{max} (Å)	N(r)
H3-O1	3.5	0.6
H3-O2	3.5	0.52
H3-O3	3.5	0.84

Fig. 7. Combined distribution function for the angle between the vectors perpendicular to the centre of neighbour rings as function of distance $d_{\#3\text{-}H6}$ (a). Geometrical organization of first HMF neighbours extrapolated considering a $d_{\#3\text{-}H6}$ between 2–3 Å and ϑ between 0–30°.

noted at distances less than 5 Å.

Fig. 3(c) provides additional insight into the mutual arrangements of neighbour rings. It reveals a notable correlation occurring at a d ~ 5 Å, with corresponding γ values falling within the range of 45–90°. By focusing on the graphical representation derived from this intense spot, we can visually discern and comprehend the structural configuration, thereby underscoring the presence of a predominant Parallel Displaced (PD) π–π stacking arrangement [58,59,68,69].

This finding is particularly intriguing as it diverges from the observations recently made for thiophene, which shares a similar molecular structure with HMF. In the case of thiophene, a perpendicular displacement occurs, with one hydrogen atom positioned directly towards the π-cloud of the ring at distances shorter than 4 Å [70].

To understand in depth the molecular and microscopic arrangements within liquid HMF, the role of the hydroxyl group was subsequently explored as an orienting moiety for the structure of the liquid. The comparison between the RDFs associated with the possible Hydrogen Bonds (HBs) between the hydroxyl hydrogen (H6) and the three oxygens (O1, O2 and O3) are shown in Fig. 4.

The peak related to the H6···O3 correlation appears quite sharp, with an amplitude larger than 2 and centered at approximately 1.9 Å. Upon integration of this peak up to 2.8 Å, the number of first neighbours is ca. 0.6. Similarly, the RDF corresponding to the H6-O2 correlation displays a sharp and intense peak, albeit with a reduced first neighbours number (roughly 0.3 for r < 2.8 Å). On the other hand, the RDF associated with correlations involving O1 are characterised by much less structured features.

One may then assume that the most relevant HB turns out to be the one involving O3 and H6, followed by the one with O2. The furan oxygen O1 is, de facto, the least efficient H-bond acceptor site, in good agreement with the low availability of the lone pairs on the O atom due to delocalization concurring to the aromaticity of the furanose ring.

This finding is confirmed through the comparison of the three CDFs, shown in Fig. 5, which are associated to the HB geometrical features (O···H distance and O-H···O angle).

Strong HB interactions can be detected, as evidenced by the presence

connecting neighbour ring centres and the vector perpendicular to the reference ring (β); c) the angle between the vectors with extremes the virtual atom #4 (Scheme 1) and ether oxygen O1 (γ), for the two neighbour rings.

Panel (a) highlights the strong correlations occurring at approximately 4.5 Å between neighbor rings arranged in a parallel (α = 0°) and antiparallel (α = 180°) alignments, which are exemplified in the figure. Related information can be extracted from panel (b); therein it emerges that at approximately 4.5 Å, the vector normal to the observed ring aligns itself either in parallel or antiparallel way to the vector connecting the two rings centers.

The structural arrangement evidenced by these CDFs prompts for the existence of π-π interactions between neighbour HMF rings. This observation resembles analogous findings from studies on other aromatic liquids, including benzene, toluene [68,69], anisole and its derivatives [58], as well as thymol [59], where a parallel alignment was
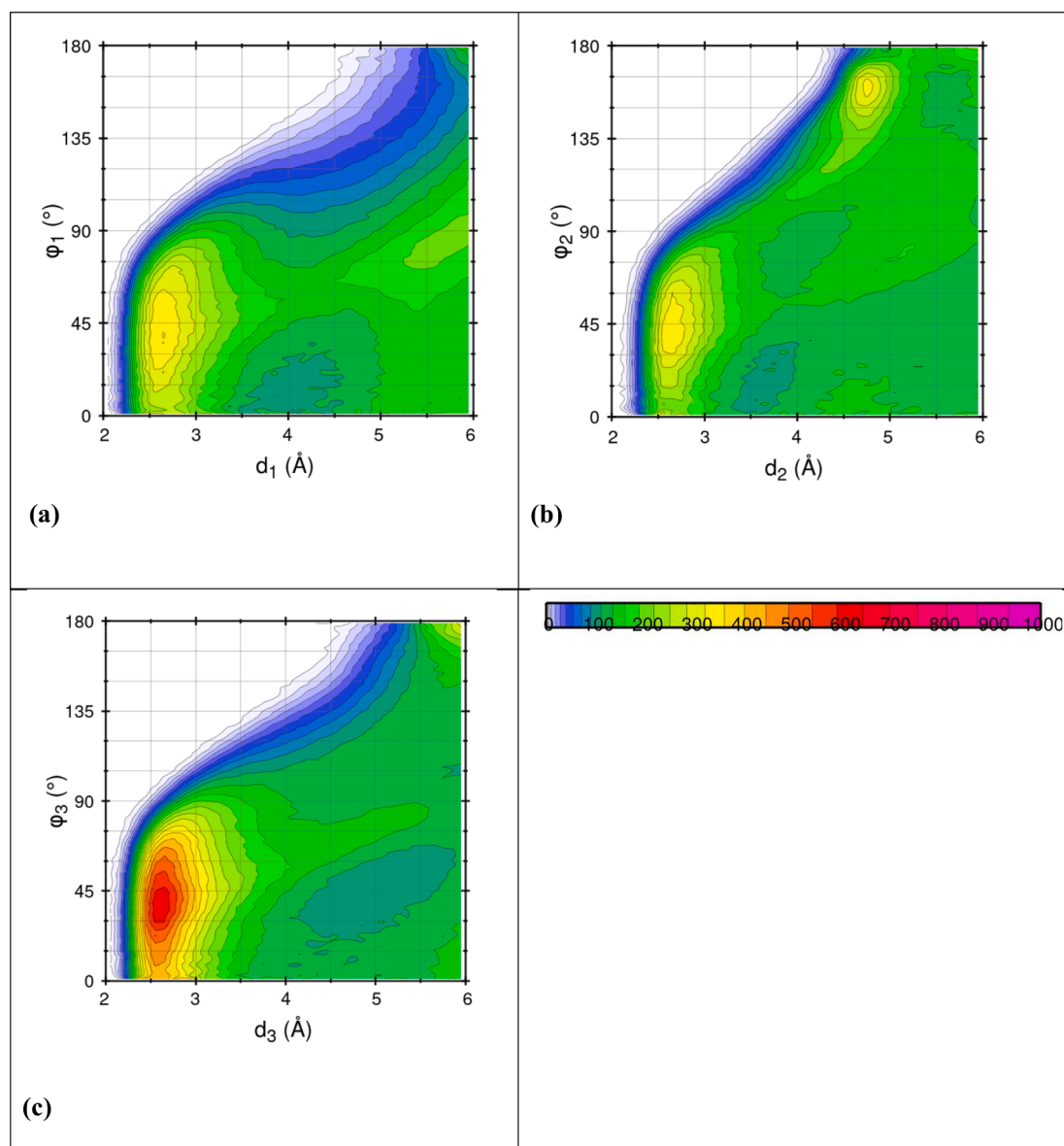
Fig. 9. Combined distribution functions for the angle C6-H3···O1 (a), C6-H3···O2 (b), and C6-H3···O3 (c) as functions of distances d_{H3-O1}, d_{H3-O2}, d_{H3-O3}, respectively.

of intense and well-defined spots centered at distances below 2 Å and at angles ϑ ranging from 0 to 30°. However, the most significant interactions pertain to the hydrogen bonding of H6 with O2 and O3, with a slight preference for H6 to participate in hydrogen bonding with O3.

We also considered the possibility of HMF hydroxyl hydrogen might be engaged in an aromatic HB (O-H···π). Fig. 6 shows the RDF associated to the H6-#3 correlation and the corresponding running neighbor numbers. The peak centered at approximately 2.4 Å has an amplitude of ca. 0.5. By integrating the RDF up to a distance of 3 Å, we determine the presence of approximately 0.2 #3 sites around H6. Given the potential importance of such an interaction, already observed in different aromatic systems [59,71,72], we explore its presence through a CDF related to the angle between vectors perpendicular to the planes of the rings (ϑ), plotted against $d_{H6-\#3}$ (Fig. 7).

The presence of significant hot spots, occurring at angles ϑ between 0° and 15° and 165° and 180°, with distances ranging between 2 and 3 Å, provides evidence that the aromatic O-H···π interaction leads to a parallel/antiparallel ring stacking. Interestingly, contrary to other systems where this interaction typically results in a perpendicular displacement between rings [59,72], here we observe a tendency for the

aromatic rings to arrange themselves in a parallel way, when interacting through the aromatic HB. This can be easily visualized through the schematic representation depicted in Fig. 7, where the parallel arrangement of rings with the O-H···π interaction bridging between them is clearly illustrated.

The role of aldehydic hydrogen (H3) in engaging interactions was also explored. Fig. 8 shows the RDFs related to the interactions of H3 with the three oxygens of the molecule.

From Fig. 8 it emerges that the most relevant feature is that related to the H3-O3 correlation, exhibiting a sharp peak centred at approximately 2.7 Å with an intensity surpassing unity. Integrating this peak up to a distance of 3.5 Å reveals approximately 0.84 O3 sites surrounding H3. H3-O1 and H3-O2 correlations display similar characteristics, with peaks centred around 2.7 Å and intensities below unity. The running neighbour numbers for all correlations depicted in Fig. 8 are summarized in Table 2.

In Fig. 9 we show CDFs associated to the geometrical features of the interactions shown in Fig. 8, in particular abscissas correspond to H3···Ox (with x = 1,2,3) distances, d_x, and the φ_x angles correspond to the angles C6-H3···Ox (with x = 1,2,3 for figures a), b) and c),
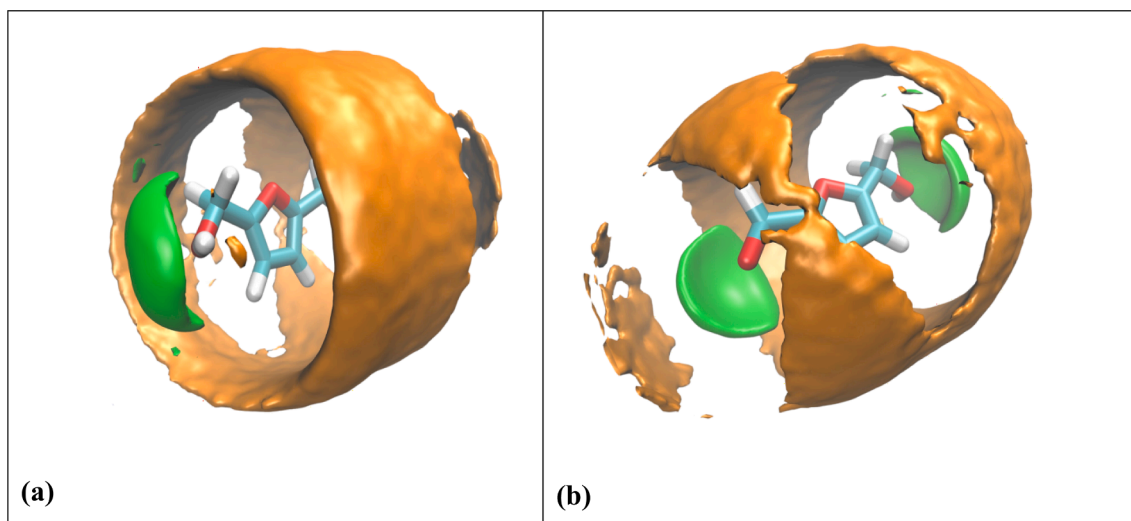
Fig. 10. Spatial distribution function of hydrogen hydroxyl (green) and centre of ring (orange) surrounding a reference HMF molecule. Distribution isovalues refer to approximately half of the maximum amplitude.
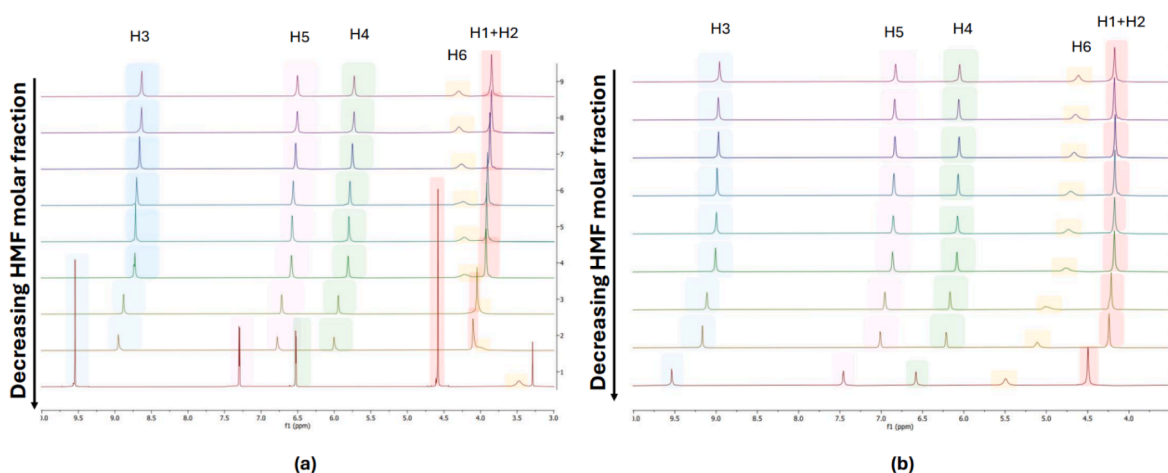

Fig. 11. (a) Stacked ^{1}H NMR spectra of pure liquid HMF (top) and liquid HMF with increasing amounts of CD$_3$CN; (b) Stacked ^{1}H NMR spectra of pure liquid HMF (top) and liquid HMF with increasing amounts of DMSO-d_6. All spectra were recorded at a temperature of 313 K. Spectral assignment is reported in the top spectra for HMF.

respectively).

Fig. 9 emphasizes that the three probed correlations are characterised by distances H3···Ox (with x = 1,2,3) ∼ 2.6 Å and angles φ_x between 30 and 45°. The H3···O3 correlation shows the strongest occurrence. These interactions are likely the consequences of other correlations that drive liquid ordering in HMF, such as the above discussed π stacking and hydrogen bonding interactions.

Fig. 10(a) and (b) depict the Spatial Distribution Functions (SDF) of HMF ring centers (orange) and hydroxyl groups (green) around a reference HMF molecule.

This visualization emphasizes the heterogeneous local structural scenario around a reference HMF: we can observe the propensity of the hydroxyl hydrogen to effectively interact with both O2 and O3 through conventional HBs, as well as the tendency of surrounding HMF molecules to engage with the reference one in a parallel manner, via a π··π stacking interaction.

The intricate structural scenario derived from the complementary use of X-ray scattering and MD data can be cross-verified using liquid-state NMR data. The synergistic use of scattering techniques (SANS, SAXS, WAXS) and NMR spectroscopy was previously demonstrated by some of us in studies involving ionic liquids [73] and eutectic mixtures [74,75].

NMR spectra are sensitive to changes in the local magnetic environment caused by intermolecular structural motifs. In structured liquids like ionic liquids and deep eutectic solvents, several NMR features can be used to monitor intermolecular interactions and interaction sites: i) individual signals in the ^{1}H spectrum can show selective chemical shift changes due to anisotropic effects like shielding/deshielding from aromatic ring currents [76,77]; ii) variations in local diamagnetic components due to the strengthening/disruption of H-bonds [78]; iii) cross-relaxation (NOE) of nuclei at interaction sites, indicating both short- and long-range effects [79,80]; and iv) translational and rotational dynamics [81]. Factors i) and ii), related to chemical shift variations due to aromatic ring currents and H-bonds, provide additional information on the correlations and intermolecular interactions in pure HMF discussed earlier. Furthermore, since the timescale of NMR spectroscopy ranges from milliseconds to seconds, the overall picture from NMR data represents a time-averaged perspective consistent with the evolution of MD frames across the entire simulation period.

Given this context, the NMR investigation strategy can be summarized as follows: in order to highlight and demonstrate the existence of π··π interactions, NMR measurements were performed on liquid HMF
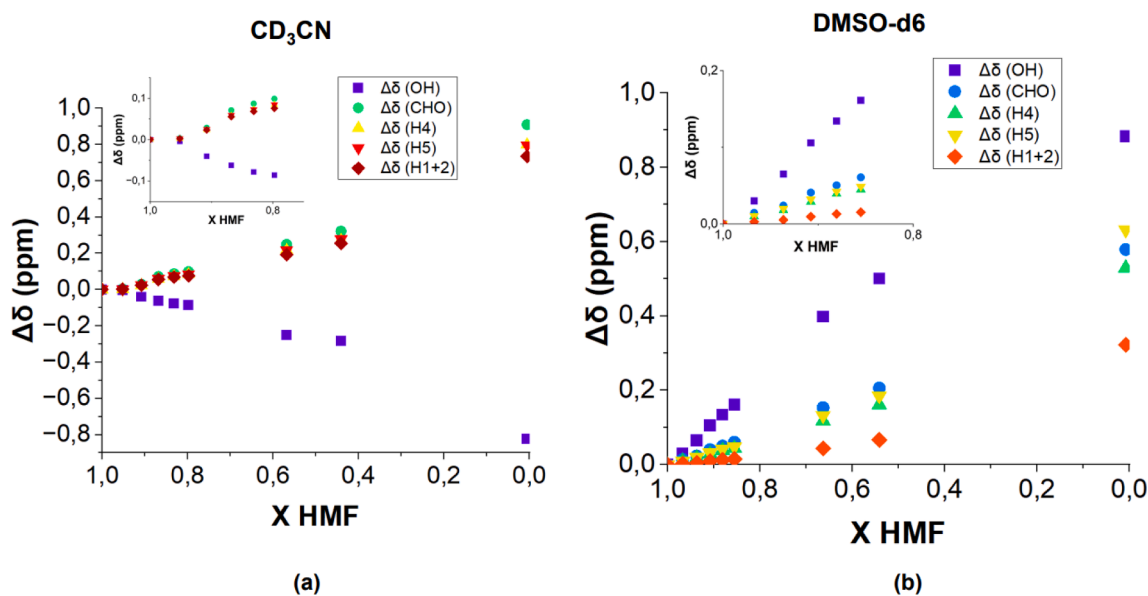
Fig. 12. (a) ^{1}H NMR shift variation of HMF signals in CD$_3$CN when decreasing the molar fraction (χ) of HMF; (b) ^{1}H NMR shift variation of HMF signals in DMSO-d_6 when decreasing the molar fraction (χ) of HMF. All spectra were recorded at a temperature of 313 K and the shifts are reported with respect to the solvent residual peak within the coaxial insert. The insets show, for clarity, the expansion of the low dilution regime.

with progressive dilution in a suitable solvent. The goal was to observe molecular correlation patterns by disrupting them through dilution. Additionally, by selecting a solvent with specific H-bond properties, one can reveal the H-bond donor sites in HMF. As such, non-interacting CD$_3$CN and strongly interacting DMSO-d_6 were chosen for chemical shift titrations. The ^{1}H NMR spectra are shown in Fig. 11, and the plots of the solvent-induced chemical shift variation $\Delta\delta$ (i.e., δ in HMF solvent minus δ in pure HMF) are depicted in Fig. 12.

Visual inspection of the spectra in both solvents (Fig. 11a) and b)) reveals a downfield shift in all signals, indicating progressive disruption of HMF $\pi\cdot\cdot\pi$ stacking caused by the solvent solvation shell, which reduces the paramagnetic effect of aromatic electrons, resulting in deshielding. Data reported in Fig. 12 confirm such a scenario, indicating a non-selective shift in all non-exchangeable protons in HMF. This is consistent with the small size of HMF, where protons H3, H4, and H6 are close enough in molecular connectivity to exhibit similar magnetic effects upon $\pi\cdot\cdot\pi$ interaction disruption. However, the behaviour of the exchangeable OH proton differs markedly between the two solvents.

In a non-interacting solvent like CD$_3$CN (Fig. 11a) and Fig. 12a)), the upfield shift of the exchangeable OH signal indicates a weakening of hydrogen bonds due to progressively increasing distance between HMF molecules. In a strong H-bond acceptor solvent like DMSO (Fig. 11b) and Fig. 12b)), the downfield shift of the exchangeable OH signal suggests deshielding of the OH proton, due to the formation of HMF··DMSO hydrogen bonds, stronger than HMF··HMF ones. Despite the disruption of $\pi\cdot\cdot\pi$ interactions with dilution, the NMR data indicate competition between HMF and DMSO for H-bond formation.

4. Conclusion

The local structural organization in liquid neat HMF has been explored by the synergic use of high energy X-ray scattering and Molecular Dynamics simulations, providing detailed insight into the structural correlations driving HMF liquid organization. HMF liquid structure, as evidenced by X-ray scattering is very well reproduced by MD simulation, which nicely accounts for the experimental data.

Among the prevailing correlations, we detected the existence of a distinct $\pi\cdot\cdot\pi$ stacking arrangement, which characterises the mutual ordering between neighbour HMF molecules. Further correlations involve hydrogen bonding between aldehyde and hydroxyl oxygen and

hydroxyl hydrogen. Furthermore, indication of the existence of OH···π hydrogen bonding interaction can be detected.

These findings underscore the complex and heterogeneous nature of the structural organization of liquid HMF.

Moreover, an NMR strategy was devised to demonstrate the existence of mutual interactions between neighbour HMF molecules and identify the associated structural motifs. Progressive dilution with molecular solvents was used, with the expectation that it would lead to predictable chemical shift variations due to the disruption of intermolecular HMF··HMF interactions. As anticipated, the paramagnetic effects of aromatic ring currents, typically linked to $\pi\cdot\cdot\pi$ stacking, were progressively reduced as solvent was added. By using CD$_3$CN and DMSO-d_6, we were able to toggle HMF··HMF hydrogen bonds, providing evidence for the role these intermolecular forces play in the local structuring of liquid HMF.

These findings provide an accurate description of microscopic structural organization liquid neat HMF. By revealing the nature of interactions taking place between the different HMF moieties, the study provides useful indication of dominant interactions that will drive HMF solvation in novel solvent media to be explored in the future.

CRediT authorship contribution statement

Giulia Adriana Bracchini: Writing – original draft, Investigation, Formal analysis. **Emanuela Mangiacapre:** Writing – original draft, Investigation, Formal analysis. **Fabrizio lo Celso:** Software, Investigation, Formal analysis. **Daniel J.M. Irving:** Investigation, Formal analysis. **Carlo Ottaviani:** Software, Investigation, Formal analysis. **Grazia Isa C. Righetti:** Writing – original draft, Investigation, Formal analysis. **Maria Enrica Di Pietro:** Writing – original draft, Investigation, Formal analysis. **Andrea Mele:** Writing – original draft, Investigation, Funding acquisition, Formal analysis, Conceptualization. **Lorenzo Guazzelli:** Writing – original draft, Funding acquisition, Conceptualization. **Olga Russina:** Writing – original draft, Investigation, Funding acquisition. **Alessandro Triolo:** Writing – review & editing, Writing – original draft, Supervision, Investigation, Funding acquisition, Formal analysis, Conceptualization.

Declaration of competing interest

Data availability

Data will be made available on request.

Acknowledgments

References

[1] Z. Zhang, J. Song, B. Han, Catalytic transformation of lignocellulose into chemicals and fuel products in ionic liquids, Chem. Rev. 117 (2017) 6834–6880, https://doi.org/10.1021/acs.chemrev.6b00457.

[2] J.J. Bozell, G.R. Petersen, Technology development for the production of biobased products from biorefinery carbohydrates—the US Department of Energy's "Top 10" revisited, Green Chem. 12 (2010) 539–554, https://doi.org/10.1039/B922014C.

[3] Y. Hu, H. Li, P. Hu, L. Li, D. Wu, Z. Xue, C. Hu, L. Zhu, Promoting the production of 5-hydroxymethylfurfural from high-concentration fructose by creating micro-reactors in a mixed solvent, Green Chem. 25 (2023) 661–670, https://doi.org/10.1039/D2GC04295A.

[4] J. Xiong, X. Lu, W. Li, S. Yang, R. Zhang, X. Li, J. Han, D. Li, Z. Yu, One-pot tandem transformation of inulin as fructose-rich platform towards 5-hydroxymethylfurfural: feedstock advantages, acid-site regulation and solvent effects, ChemSusChem 16 (2023) e202201936, https://doi.org/10.1002/cssc.202201936.

[5] M. Zuo, X. Wang, Q. Wang, X. Zeng, L. Lin, Aqueous-natural deep eutectic solvent-enhanced 5-hydroxymethylfurfural production from glucose, starch, and food wastes, ChemSusChem 15 (2022) e202101889, https://doi.org/10.1002/cssc.202101889.

[6] H. Chang, I. Bajaj, A.H. Motagamwala, A. Somasundaram, G.W. Huber, C.T. Maravelias, J.A. Dumesic, Sustainable production of 5-hydroxymethyl furfural from glucose for process integration with high fructose corn syrup infrastructure, Green Chem. 23 (2021) 3277–3288, https://doi.org/10.1039/D1GC00311A.

[7] Q. Hou, X. Qi, M. Zhen, H. Qian, Y. Nie, C. Bai, S. Zhang, X. Bai, M. Ju, Biorefinery roadmap based on catalytic production and upgrading 5-hydroxymethylfurfural, Green Chem. 23 (2021) 119–231, https://doi.org/10.1039/D0GC02770G.

[8] C. Rosenfeld, J. Konnerth, W. Sailer-Kronlachner, P. Solt, T. Rosenau, H.W.G. van Herwijnen, Current situation of the challenging scale-up development of hydroxymethylfurfural production, ChemSusChem 13 (2020) 3544–3564, https://doi.org/10.1002/cssc.202000581.

[9] S. Marullo, F. D'Anna, The role played by ionic liquids in carbohydrates conversion into 5-hydroxymethylfurfural: a recent overview, Molecules 27 (2022) 24, https://doi.org/10.3390/molecules27072210.

[10] H. Montes-Campos, T. Méndez-Morales, L.M. Varela, M.A. Ortuño, Role of anions in 5-hydroxymethylfurfural solvation in ionic liquids from molecular dynamics simulations, Adv. Theory. Simul. 5 (2022) 2200522, https://doi.org/10.1002/adts.202200522.

[11] J. Esteban, A.J. Vorholt, W. Leitner, An overview of the biphasic dehydration of sugars to 5-hydroxymethylfurfural and furfural: a rational selection of solvents using COSMO-RS and selection guides, Green Chem. 22 (2020) 2097–2128, https://doi.org/10.1039/C9GC04208C.

[12] F. Ilgen, D. Ott, D. Kralisch, C. Reil, A. Palmberger, B. König, Conversion of carbohydrates into 5-hydroxymethylfurfural in highly concentrated low melting mixtures, Green Chem. 11 (2009) 1948–1954, https://doi.org/10.1039/B917548M.

[13] G.R. Gomes, J.C. Pastre, Microwave-assisted HMF production from water-soluble sugars using betaine-based natural deep eutectic solvents (NADES), Sustain. Energy Fuels 4 (2020) 1891–1898, https://doi.org/10.1039/C9SE01278H.

[14] L. Chen, Y. Xiong, H. Qin, Z. Qi, Advances of ionic liquids and deep eutectic solvents in green processes of biomass-derived 5-hydroxymethylfurfural, ChemSusChem 15 (2022) e202102635, https://doi.org/10.1002/cssc.202102635.

[15] M. Li, H. Jiang, L. Zhang, X. Yu, H. Liu, A.E.A. Yagoub, C. Zhou, Synthesis of 5-HMF from an ultrasound-ionic liquid pretreated sugarcane bagasse by using a microwave-solid acid/ionic liquid system, Ind. Crops Prod. 149 (2020) 112361, https://doi.org/10.1016/j.indcrop.2020.112361.

[16] H. Guo, X. Qi, Deep eutectic solvents for synthesis of 5-hydroxymethylfurfural, Curr. Opin. Green Sustain. Chem. 47 (2024) 100924, https://doi.org/10.1016/j.cogsc.2024.100924.

[17] W. Fan, C. Verrier, Y. Queneau, F. Popowycz, 5-Hydroxymethylfurfural (HMF) in organic synthesis: a review of its recent applications towards fine chemicals, Curr. Org. Synth. 16 (2019) 583–614, https://doi.org/10.2174/1570179416666190412164738.

[18] K.I. Galkin, V.P. Ananikov, When will 5-hydroxymethylfurfural, the "sleeping giant" of sustainable chemistry, awaken? ChemSusChem 12 (2019) 2976–2982, https://doi.org/10.1002/cssc.201900592.

[19] M. Bicker, J. Hirth, H. Vogel, Dehydration of fructose to 5-hydroxymethylfurfural in sub- and supercritical acetone, Green Chem. 5 (2003) 280–284, https://doi.org/10.1039/B211468B.

[20] X. Tong, Y. Ma, Y. Li, Biomass into chemicals: Conversion of sugars to furan derivatives by catalytic processes, Appl. Catal. A Gen. 385 (2010) 1–13, https://doi.org/10.1016/j.apcata.2010.06.049.

[21] F.H. Isikgor, C.R. Becer, Lignocellulosic biomass: a sustainable platform for the production of bio-based chemicals and polymers, Polym. Chem. 6 (2015) 4497–4559, https://doi.org/10.1039/C5PY00263J.

[22] Z. Jiang, Y. Zeng, D. Hu, R. Guo, K. Yan, R. Luque, Chemical transformations of 5-hydroxymethylfurfural into highly added value products: present and future, Green Chem. 25 (2023) 871–892, https://doi.org/10.1039/D2GC03444A.

[23] D. Rigo, D. Polidoro, A. Perosa, M. Selva, Diversified upgrading of HMF via acetylation, aldol condensation, carboxymethylation, vinylation and reductive amination reactions, Mol. Catal. 514 (2021) 111838, https://doi.org/10.1016/j.mcat.2021.111838.

[24] W. Ramdani, I. Rabadán González, N. Benbakoura, M. Ahmar, C. Verrier, Y. Queneau, M. Pera-Titus, F. Jérôme, K. De Oliveira Vigier, Catalytic aldol condensation of 5-hydroxymethylfurfural and its synthesis from concentrated feed of carbohydrates, ChemCatChem 15 (2023) e202300044, https://doi.org/10.1002/cctc.202300044.

[25] F.A. Kucherov, K.I. Galkin, E.G. Gordeev, V.P. Ananikov, Efficient route for the construction of polycyclic systems from bioderived HMF, Green Chem. 19 (2017) 4858–4864, https://doi.org/10.1039/C7GC02211E.

[26] H. Chang, G.W. Huber, J.A. Dumesic, Chemical-switching strategy for synthesis and controlled release of norcantharimides from a biomass-derived chemical, ChemSusChem 13 (2020) 5213–5219, https://doi.org/10.1002/cssc.202001471.

[27] V.R. Elías, G.O. Ferrero, M.G. Idriceanu, G.A. Eimer, M.E. Domine, From biomass-derived furans to aromatic compounds: design of Al–Nb-SBA-15 mesoporous structures and study of their acid properties on catalytic performance, Catal. Sci. Technol. 14 (2024) 1488–1500, https://doi.org/10.1039/D4CY00033A.

[28] S. Zheng, Z. Wei, B. Wozniak, F. Kallmeier, E. Baráth, H. Jiao, S. Tin, J.G. de Vries, Synthesis of valuable benzenoid aromatics from bioderived feedstock, Nat. Sustain. 6 (2023) 1436–1445, https://doi.org/10.1038/s41893-023-01190-w.

[29] J.C. Velasco Calderón, J.S. Arora, S.H. Mushrif, Mechanistic investigation into the formation of humins in acid-catalyzed biomass reactions, ACS Omega 7 (2022) 44786–44795, https://doi.org/10.1021/acsomega.2c04783.

[30] A. Wassenberg, T. Esser, M.J. Poller, J. Albert, Investigation of the formation, characterization, and oxidative catalytic valorization of humins, Materials 16 (2023) 2864, https://doi.org/10.3390/ma16072864.

[31] L. Shuai, J. Luterbacher, Organic solvent effects in biomass conversion reactions, ChemSusChem 9 (2016) 133–155, https://doi.org/10.1002/cssc.201501148.

[32] X. Fu, Y. Hu, Y. Zhang, Y. Zhang, D. Tang, L. Zhu, C. Hu, Solvent effects on degradative condensation side reactions of fructose in its initial conversion to 5-hydroxymethylfurfural, ChemSusChem 13 (2020) 501–512, https://doi.org/10.1002/cssc.201902309.

[33] N. Rodriguez Quiroz, T.-H. Chen, T.-Y. Chen, S. Caratzoulas, D.G. Vlachos, Unexpected kinetic solvent effects enhance activity and selectivity in biphasic systems, ACS Catal. 13 (2023) 7942–7954, https://doi.org/10.1021/acscatal.3c00894.

[34] C. Sanpitakseree, A.H. Motagamwala, J.A. Dumesic, M. Neurock, Solvent and chloride ion effects on the acid-catalyzed conversion of glucose to 5-hydroxymethylfurfural, ACS Sustain. Chem. Eng. 10 (2022) 8275–8288, https://doi.org/10.1021/acssuschemeng.2c00651.

[35] G. Tsilomelekis, T.R. Josephson, V. Nikolakis, S. Caratzoulas, Origin of 5-hydroxymethylfurfural stability in water/dimethyl sulfoxide mixtures, ChemSusChem 7 (2014) 117–126, https://doi.org/10.1002/cssc.201300786.

[36] C. Sepali, S. Skoko, L. Guglielmero, T. Giovannini, A. Mezzetta, F. D'Andrea, C.S. Pomelli, L. Guazzelli, C. Cappelli, Deciphering the structure of deep eutectic solvents: a computational study from the solute's viewpoint, J. Mol. Liq. 399 (2024) 124326, https://doi.org/10.1016/j.molliq.2024.124326.

[37] S.H. Mushrif, S. Caratzoulas, D.G. Vlachos, Understanding solvent effects in the selective conversion of fructose to 5-hydroxymethyl-furfural: a molecular dynamics investigation, Phys. Chem. Chem. Phys. 14 (2012) 2637–2644, https://doi.org/10.1039/C2CP22694D.

[38] F. Grote, I. Ermilova, A.P. Lyubartsev, Molecular dynamics simulations of furfural and 5-hydroxymethylfurfural at ambient and hydrothermal conditions, J. Phys. Chem. B 122 (2018) 8416–8428, https://doi.org/10.1021/acs.jpcb.8b03350.

[39] S. Rabet, G. Raabe, Comparison of the GAFF, OPLSAA and CHARMM27 force field for the reproduction of the thermodynamics properties of furfural, 2-methylfuran, 2,5-dimethylfuran and 5-hydroxymethylfurfural, Fluid Phase Equilib. 554 (2022) 113331, https://doi.org/10.1016/j.fluid.2021.113331.

[40] S. Jha, P. Sappidi, Molecular simulations of understanding the structure and separation thermodynamics of 5-Hydroxymethylfurfural from 1-Butyl-3-Methyl imidazolium tetrafluoroborate, J. Mol. Liq. 391 (2023) 123354, https://doi.org/10.1016/j.molliq.2023.123354.

[41] O. Russina, F. Lo Celso, N.V. Plechkova, A. Triolo, Emerging evidences of mesoscopic-scale complexity in neat ionic liquids and their mixtures, J. Phys. Chem. Lett. 8 (2017) 1197–1204, https://doi.org/10.1021/acs.jpclett.6b02811.

[42] M. Basham, J. Filik, M.T. Wharmby, P.C.Y. Chang, B. El Kassaby, M. Gerring, J. Aishima, K. Levik, B.C.A. Pulford, I. Sikharulidze, D. Sneddon, M. Webber, S. S. Dhesi, F. Maccherozzi, O. Svensson, S. Brockhauser, G. Náray, A.W. Ashton, Data analysis WorkbeNch (DAWN), J. Synchrotron Radiat. 22 (2015) 853–858, https://doi.org/10.1107/S1600577515002283.

[43] A.K. Soper, GudrunN and GudrunX: programs for correcting raw neutron and X-ray diffraction data to differential scattering cross section, 2011. http://epubs.stfc.ac.uk.

[44] B. Hess, C. Kutzner, D. Van Der Spoel, E. Lindahl, GROMACS 4: algorithms for highly efficient, load-balanced, and scalable molecular simulation, J. Chem. Theory Comput. 4 (2008) 435–447, https://doi.org/10.1021/ct700301q.

[45] D. Van Der Spoel, E. Lindahl, B. Hess, G. Groenhof, A.E. Mark, H.J.C. Berendsen, GROMACS: fast, flexible, and free, J. Comput. Chem. 26 (2005) 1701–1718, https://doi.org/10.1002/jcc.20291.

[46] W.L. Jorgensen, D.S. Maxwell, J. Tirado-Rives, Development and testing of the OPLS all-atom force field on conformational energetics and properties of organic liquids, J. Am. Chem. Soc. 118 (1996) 11225–11236. https://pubs.acs.org/sharingguidelines.

[47] W.L. Jorgensen, J. Tirado-Rives, Potential energy functions for atomic-level simulations of water and organic and biomolecular systems, Proc. Natl. Acad. Sci. 102 (2005) 6665–6670, https://doi.org/10.1073/pnas.0408037102.

[48] L.S. Dodda, J.Z. Vilseck, J. Tirado-Rives, W.L. Jorgensen, 1.14*CM1A-LBCC: localized bond-charge corrected CM1A charges for condensed-phase simulations, J. Phys. Chem. B 121 (2017) 3864–3870, https://doi.org/10.1021/acs.jpcb.7b00272.

[49] L.S. Dodda, I.C. De Vaca, J. Tirado-Rives, W.L. Jorgensen, LigParGen web server: an automatic OPLS-AA parameter generator for organic ligands, Nucl. Acids Res. 45 (2017) W331–W336, https://doi.org/10.1093/nar/gkx312.

[50] L. Martinez, R. Andrade, E.G. Birgin, J.M. Martínez, PACKMOL: a package for building initial configurations for molecular dynamics simulations, J. Comput. Chem. 30 (2009) 2157–2164, https://doi.org/10.1002/jcc.21224.

[51] G. Bussi, D. Donadio, M. Parrinello, Canonical sampling through velocity rescaling, J. Chem. Phys. 126 (2007) 014101, https://doi.org/10.1063/1.2408420.

[52] M. Parrinello, A. Rahman, Polymorphic transitions in single crystals: a new molecular dynamics method, J. Appl. Phys. 52 (1981) 7182–7190, https://doi.org/10.1063/1.328693.

[53] T. Darden, D. York, L. Pedersen, Particle mesh Ewald: An N·log(N) method for Ewald sums in large systems, J. Chem. Phys. 98 (1993) 10089–10092, https://doi.org/10.1063/1.464397.

[54] U. Essmann, L. Perera, M.L. Berkowitz, T. Darden, H. Lee, L.G. Pedersen, A smooth particle mesh Ewald method, J. Chem. Phys. 103 (1995) 8577–8593, https://doi.org/10.1063/1.470117.

[55] M. Brehm, B. Kirchner, TRAVIS – a free analyzer and visualizer for Monte Carlo and molecular dynamics trajectories, J. Chem. Inf. Model 51 (2011) 2007–2023, https://doi.org/10.1021/ci200217w.

[56] O. Hollóczki, M. Macchiagodena, H. Weber, M. Thomas, M. Brehm, A. Stark, O. Russina, A. Triolo, B. Kirchner, Triphilic ionic-liquid mixtures: fluorinated and non-fluorinated aprotic ionic-liquid mixtures, ChemPhysChem 16 (2015) 3325–3333, https://doi.org/10.1002/cphc.201500473.

[57] M. Brehm, M. Thomas, S. Gehrke, B. Kirchner, TRAVIS—a free analyzer for trajectories from molecular simulation, J. Chem. Phys. 152 (2020) 164105, https://doi.org/10.1063/5.0005078.

[58] A. Triolo, F. Lo Celso, N.V. Plechkova, F. Leonelli, S. Gärtner, D.S. Keeble, O. Russina, Structure of anisole derivatives by total neutron and X-ray scattering: Evidences of weak C-H⋯O and C-H⋯π interactions in the liquid state, J. Mol. Liq. 314 (2020) 113795, https://doi.org/10.1016/j.molliq.2020.113795.

[59] E. Mangiacapre, A. Triolo, F. Ramondo, F. Lo Celso, O. Russina, Unveiling the structural organisation of carvacrol through X-ray scattering and molecular Dynamics: a comparative study with liquid thymol, J. Mol. Liq. 394 (2024) 123778, https://doi.org/10.1016/j.molliq.2023.123778.

[60] W. Xu, E.I. Cooper, C.A. Angell, Ionic liquids: Ion mobilities, glass temperatures, and fragilities, J. Phys. Chem. B 107 (2003) 6170–6178, https://doi.org/10.1021/jp0275894.

[61] S.R. Elliott, The origin of the first sharp diffraction peak in the structure factor of covalent glasses and liquids, J. Phys.: Condensed Matter 4 (1992) 7661, https://doi.org/10.1088/0953-8984/4/38/003.

[62] O. Russina, A. Triolo, L. Gontrani, R. Caminiti, Mesoscopic structural heterogeneities in room-temperature ionic liquids, J. Phys. Chem. Lett. 3 (2012) 27–33, https://doi.org/10.1021/jz201349z.

[63] A. Triolo, O. Russina, H.J. Bleif, E. Di Cola, Nanoscale segregation in room temperature ionic liquids, J. Phys. Chem. B 111 (2007) 4641–4644, https://doi.org/10.1021/jp067705t.

[64] N. Schaeffer, D.O. Abranches, L.P. Silva, M.A.R. Martins, P.J. Carvalho, O. Russina, A. Triolo, L. Paccou, Y. Guinet, A. Hedoux, J.A.P. Coutinho, Non-ideality in thymol + menthol type v deep eutectic solvents, ACS Sustain. Chem. Eng. 9 (2021) 2203–2211, https://doi.org/10.1021/acssuschemeng.0c07874.

[65] A. Malik, H.K. Kashyap, Origin of structural and dynamic heterogeneity in thymol and coumarin-based hydrophobic deep eutectic solvents as revealed by molecular dynamics, Phys. Chem. Chem. Phys. 25 (2023) 19693–19705, https://doi.org/10.1039/d3cp01770b.

[66] A. Malik, H.K. Kashyap, Heterogeneity in hydrophobic deep eutectic solvents: SAXS prepeak and local environments, Phys. Chem. Chem. Phys. 23 (2021) 3915–3924, https://doi.org/10.1039/d0cp05407k.

[67] A. Triolo, F. Lo Celso, O. Russina, Liquid structure of a water-based, hydrophobic and natural deep eutectic solvent: the case of thymol-water. A Molecular Dynamics study, J. Mol. Liq. 372 (2023) 121151, https://doi.org/10.1016/j.molliq.2022.121151.

[68] T.F. Headen, C.A. Howard, N.T. Skipper, M.A. Wilkinson, D.T. Bowron, A.K. Soper, Structure of π−π interactions in aromatic liquids, J. Am. Chem. Soc. 132 (2010) 5735–5742, https://doi.org/10.1021/ja909084e.

[69] M. Falkowska, D.T. Bowron, H.G. Manyar, C. Hardacre, T.G.A. Youngs, Neutron scattering of aromatic and aliphatic liquids, ChemPhysChem (2016) 2043–2055, https://doi.org/10.1002/cphc.201600149.

[70] T.F. Headen, C. Di Mino, T.G. Youngs, A.J. Clancy, The structure of liquid thiophene from total neutron scattering, Phys. Chem. Chem. Phys. 25 (2023) 25157–25165, https://doi.org/10.1039/d3cp03932c.

[71] M.W. Johnson, Neutron Scattering Data Analysis 1990: Invited and Contributed Papers from the Conference on Neutron Scattering Data Analysis held at the Rutherford Appleton Laboratory, Institute of Physics, 1990.

[72] C. Di Mino, A.G. Seel, A.J. Clancy, T.F. Headen, T. Földes, E. Rosta, A. Sella, N. T. Skipper, Strong structuring arising from weak cooperative O-H⋯π and C-H⋯O hydrogen bonding in benzene-methanol solution, Nat. Commun. 14 (2023) 5900, https://doi.org/10.1038/s41467-023-41451-y.

[73] F. Lo Celso, Y. Yoshida, F. Castiglione, M. Ferro, A. Mele, C.J. Jafta, A. Triolo, O. Russina, Direct experimental observation of mesoscopic fluorous domains in fluorinated room temperature ionic liquids, Phys. Chem. Chem. Phys. 19 (2017) 13101–13110, https://doi.org/10.1039/C7CP01971H.

[74] A. Triolo, M.E. Di Pietro, A. Mele, F. Lo Celso, M. Brehm, V. Di Lisio, A. Martinelli, P. Chater, O. Russina, Liquid structure and dynamics in the choline acetate:urea 1:2 deep eutectic solvent, J. Chem. Phys. 154 (2021) 244501, https://doi.org/10.1063/5.0054048.

[75] E. Mangiacapre, F. Castiglione, M. D'Aristotile, V. Di Lisio, A. Triolo, O. Russina, Choline chloride-water mixtures as new generation of green solvents: a comprehensive physico-chemical study, J. Mol. Liq. 383 (2023) 122120, https://doi.org/10.1016/j.molliq.2023.122120.

[76] X. Liu, A. Mariani, T. Diemant, M.E. Di Pietro, X. Dong, M. Kuenzel, A. Mele, S. Passerini, Difluorobenzene-based locally concentrated ionic liquid electrolyte enabling stable cycling of lithium metal batteries with nickel-rich cathode, Adv. Energy Mater. 12 (2022) 2200862, https://doi.org/10.1002/aenm.202200862.

[77] C. Xu, T. Diemant, A. Mariani, M.E. Di Pietro, A. Mele, X. Liu, S. Passerini, Locally concentrated ionic liquid electrolytes for wide-temperature-range aluminum-sulfur batteries, Angew. Chem. Int. Ed. 63 (2024) e202318204, https://doi.org/10.1002/anie.202318204.

[78] M. Busato, G. Mannucci, L.A. Rocchi, M.E. Di Pietro, A. Capocefalo, E. Zorzi, P. Casu, D. Veclani, F. Castiglione, A. Mele, A. Martinelli, P. Postorino, P. D'Angelo, The complex story behind a deep eutectic solvent formation as revealed by l-menthol mixtures with butylated hydroxytoluene derivatives, ACS Sustain. Chem. Eng. 11 (2023) 8988–8999, https://doi.org/10.1021/acssuschemeng.3c01209.

[79] P. Honegger, M.E. Di Pietro, F. Castiglione, C. Vaccarini, A. Quant, O. Steinhauser, C. Schröder, A. Mele, The intermolecular NOE depends on isotope selection: short range vs long range behavior, J. Phys. Chem. Lett. 12 (2021) 8658–8663, https://doi.org/10.1021/acs.jpclett.1c02253.

[80] M.E. Di Pietro, K. Goloviznina, A. van den Bruinhorst, G. de Araujo Lima e Souza, M. Costa Gomes, A.A.H. Padua, A. Mele, Lithium salt effects on the liquid structure of choline chloride-urea deep eutectic solvent, ACS Sustain. Chem. Eng. 10 (2022) 11835–11845, https://doi.org/10.1021/acssuschemeng.2c02460.

[81] G. de Araujo Lima e Souza, M.E. Di Pietro, F. Castiglione, P. Fazzio Martins Martinez, M. Middendorf, M. Schönhoff, C.C. Fraenza, P. Stallworth, S. Greenbaum, A. Triolo, G.B. Appetecchi, A. Mele, Unveiling the transport properties of protic ionic liquids: lithium ion dynamics modulated by the anion fluorine reservoir, Electrochim. Acta 475 (2024) 143598, https://doi.org/10.1016/j.electacta.2023.143598.